

BEC-BCS Crossover in Neutron Matter with Renormalization Group based Effective Interactions

S. Ramanan*

Department of Physics, Indian Institute of Technology Madras, Chennai - 600036, India

M. Urban†

Institut de Physique Nucléaire, CNRS-IN2P3 and Université Paris-Sud, 91406 Orsay Cedex, France

We study pure neutron matter in the BEC-BCS crossover regime using renormalization group based low-momentum interactions within the Nozières-Schmitt-Rink framework. This is an attempt to go beyond the mean field description for low-density matter. We work in the basis of so-called Weinberg eigenvectors where the operator G_0V is diagonal, which proves to be an excellent choice that allows one to use non-local interactions in a very convenient way. We study the importance of correlations as a function of density. We notice that there is a significant reduction of the BCS critical temperature at low-densities as the neutron matter approaches the unitary limit.

PACS numbers: 21.65.Cd

I. INTRODUCTION

The study of pairing correlations between nucleons is important for both infinite matter such as neutron stars as well as for finite nuclei, especially close to the drip lines [1–8]. In neutron matter at low density, strong correlations build up between the interacting pair of neutrons due to weak Pauli-blocking [2]. Evidence for such correlations have been observed in nuclei close to the drip lines, for example in ^{11}Li where the two neutrons outside the core become strongly correlated [5–8]. In addition to playing a crucial role in halo nuclei, strong correlations are important to explain the glitches as well as the cooling rates of neutron stars [3, 4]. Typically a neutron star, which is born at the end of a core collapse supernova, consists of asymmetric nuclear matter, i.e. neutrons and protons in β equilibrium with the electrons. In the inner crust, protons and neutrons form clusters that are surrounded by a superfluid neutron gas.

In this paper we study pure neutron matter and analyze the pairing correlations as a function of density. In symmetric matter at low density, one expects a Bose-Einstein condensate (BEC) of deuterons [9–11], but in pure neutron matter, low density does not lead to a BEC state, because there is no bound di-neutron state. Nevertheless it results in matter being strongly correlated. In fact, at low densities neutron matter tends almost to a unitary gas as introduced by Bertsch [12] because of the unusually large neutron-neutron scattering length of ≈ -18.7 fm [13]. At higher density, the pair correlations become less important and the system can be described within Bardeen-Cooper-Schrieffer (BCS) mean-field theory. Pairing in neutron matter has been widely studied within the BCS theory (for an overview, see, e.g.,

Chapter 8.2 of [14]), but in the strongly correlated regime the transition temperature T_c is strongly overestimated within this approach. In order to go beyond the mean field approximation, we need to include pair correlations above T_c . The Nozières-Schmitt-Rink (NSR) approach involves the inclusion of two-particle correlations into the density above T_c within the ladder approximation [15]. At higher density, a very similar approach by the Rostock group [9, 10], building the ladder diagrams out of quasiparticles instead of free particles, seems to be more adequate.

In the present work, we will use renormalization group based effective interactions ($V_{\text{low } k}$) as the two-body input (for a recent review, we refer the reader to [16]). Such interactions were already employed to describe pairing in finite nuclei and infinite matter [17–19]. They allow for a model independent approach to the nuclear many-body problem and one can use the residual dependence on the renormalization scale as a tool to get an estimate of the missing many-body physics. These interactions are non-local. For a general potential V , the magnitude of the eigenvalues of the operator G_0V , where G_0 is the two-body Green's function, quantifies the convergence of a Born series expansion of the T matrix. If there are sources of non-perturbative physics, these show up in the so-called Weinberg eigenvalues of this operator [20, 21, 23]. For example, in free space a bound state corresponds to a pole in the T matrix. The Weinberg eigenvalue equation for the operator G_0V at the binding energy is just the Schrödinger equation for a bound state and hence the eigenvalue equals 1. In the many-body system, the formation of Cooper pairs is very similar to the formation of bound states. This idea has been previously used to obtain the BCS pairing gap by looking at the eigenvalues crossing 1 close to the Fermi surface [23]. In this paper we generalize this idea to finite temperature, which is the Thouless criterion for the onset of pairing [15, 24, 25]. In addition to obtaining the transition temperature, the basis where the operator G_0V is diago-

*Electronic address: suna@physics.iitm.ac.in

†Electronic address: urban@ipno.in2p3.fr

nal offers additional simplification for the calculation of the correlated density.

This paper has been organized as follows. In section II we discuss the finite-temperature generalization for the Weinberg eigenvalue equation and use the eigenvalues to calculate the BCS critical temperature. In section III we obtain a formula for the correlated density within the NSR approach. We present our results in section IV and discuss the critical temperature as a function of density and we discuss the implications of our results for the understanding of pairing correlations in low-density neutron matter. In section V, we summarize and give an outlook to improvements of the theory that should be addressed in future studies.

To simplify the notation, we use units with $\hbar = c = m = k_B = 1$, where \hbar is the reduced Planck constant, c is the speed of light, m is the neutron mass, and k_B is the Boltzmann constant. To convert energies from fm^{-2} into MeV one therefore has to multiply them by $\hbar^2/m = 41.44 \text{ MeV fm}^2$, and to convert momenta from fm^{-1} into MeV one has to use $\hbar c = 197.3 \text{ MeV fm}$.

II. FINITE-TEMPERATURE EIGENVALUES AND CRITICAL TEMPERATURE

In this study we are interested in the transition from the normal to the paired state. The critical temperature that determines the on-set of pairing correlations can be obtained by the Thouless criterion, which states that if the T matrix does not exhibit a pole, the temperature is above the superfluid transition temperature [24, 25]. Therefore we look for the poles of the in-medium finite-temperature T matrix. We do this using the eigenvalues of the operator G_0V , where G_0 is the non-interacting two-body Green's function [20, 21, 23].

Let us briefly show how this works in free space. We begin by considering for a given energy E a basis $\{|\Gamma(E)\rangle\}$ such that the operator $G_0(E)V$ is diagonal, i.e.,

$$G_0(E)V|\Gamma(E)\rangle = \eta(E)|\Gamma(E)\rangle, \quad (1)$$

where $\eta(E)$ is the eigenvalue [20, 21, 26]. The form of the Green's function determines the properties of the eigenvalue. In free space at zero temperature, for example, we have $G_0(E) = (E - H_0)^{-1} = (E - K^2/4 - q^2)^{-1}$, where H_0 is the non-interacting hamiltonian and K and q are the total and relative momenta of the two particles, respectively. Then the eigenvalues are complex for positive energies (to be precise, for $E > K^2/4$) and real for negative energies. The eigenvalue equation (1) can be inverted to yield the Schrödinger equation:

$$\left(H_0 + \frac{V}{\eta(E)}\right)|\Gamma\rangle = E|\Gamma\rangle. \quad (2)$$

Therefore the eigenvalues have another interpretation: it is the factor by which the potential should be scaled in order to support a bound state at the given energy E . If

the potential does allow a bound state at an energy E_b , then the corresponding eigenvalue $\eta(E_b)$ equals 1.

In [21, 22], the eigenvalues were used as a diagnostic to track the ‘‘perturbativeness’’ of the particle-particle ladders, both in free space and in-medium, when the renormalization group based interactions $V_{\text{low } k}$ were used as inputs, and [23] extended the eigenvalue framework to study pairing at zero temperature. Since we need the transition temperature, the first step is to generalize the eigenvalue equation (1) to finite temperature $T = 1/\beta$.

We will use the Matsubara (imaginary time) formalism [27], in which the non-interacting single-particle Green's function is given by

$$\mathcal{G}_0^{(1)}(\mathbf{k}, \omega_n) = \frac{1}{i\omega_n - \epsilon_{\mathbf{k}} + \mu}, \quad (3)$$

where $\omega_n = (2n + 1)\pi/\beta$ is a fermionic Matsubara frequency and $\epsilon_{\mathbf{k}}$ is the single-particle energy. The corresponding two-body Green's function is obtained from

$$\begin{aligned} \mathcal{G}_0^{(2)}(\mathbf{K}, \mathbf{q}, \omega_N) = & -\frac{1}{\beta} \sum_{\omega_n} \mathcal{G}_0^{(1)}\left(\frac{\mathbf{K}}{2} + \mathbf{q}, \omega_n\right) \\ & \times \mathcal{G}_0^{(1)}\left(\frac{\mathbf{K}}{2} - \mathbf{q}, \omega_N - \omega_n\right) \end{aligned} \quad (4)$$

where $\omega_N = 2\pi N/\beta$ is a bosonic Matsubara frequency. Using standard techniques [27] one can perform the sum over ω_n , and the retarded two-body Green's function at finite density and temperature for real energy ω is obtained by analytic continuation, $i\omega_N \rightarrow \omega + i\eta$:

$$G_0(\mathbf{K}, \mathbf{q}, \omega) = \frac{1 - f(\xi_{\mathbf{K}/2+\mathbf{q}}) - f(\xi_{\mathbf{K}/2-\mathbf{q}})}{\omega - \xi_{\mathbf{K}/2+\mathbf{q}} - \xi_{\mathbf{K}/2-\mathbf{q}} + i\eta}. \quad (5)$$

where $f(\xi) = 1/(e^{\beta\xi} + 1)$ is the Fermi-Dirac distribution function and $\omega = E - 2\mu$, $\xi_{\mathbf{k}} = \epsilon_{\mathbf{k}} - \mu$ are the energies measured from the chemical potential.

Working in momentum space in a partial wave basis, and considering only the 1S_0 channel, we can write the generalization of the eigenvalue equation to finite temperature as follows:

$$\begin{aligned} \frac{2}{\pi} \int_0^{q_{\text{max}}} dq' q'^2 v(q, q') \overline{G}_0(K, q', \omega) \Gamma(q', K, \omega) \\ = \eta(K, \omega) \Gamma(q, K, \omega), \end{aligned} \quad (6)$$

where $v(q, q')$ is the matrix element of the interaction in the 1S_0 channel and \overline{G}_0 is the angle average of G_0 . Note that in equation (6) we solve for VG_0 instead of G_0V in equation (1) analogous to [21, 23]. Both operators have the same eigenvalue spectrum, but the choice VG_0 is more convenient in numerical calculations since it allows for direct integration over singularities. In the case of a free particle spectrum, $\epsilon_{\mathbf{k}} = k^2/2$, the angle average can be done analytically with the result

$$\overline{G}_0(K, q, \omega) = \frac{\overline{Q}(K, q)}{\omega + 2\mu - K^2/4 - q^2 + i\eta}, \quad (7)$$

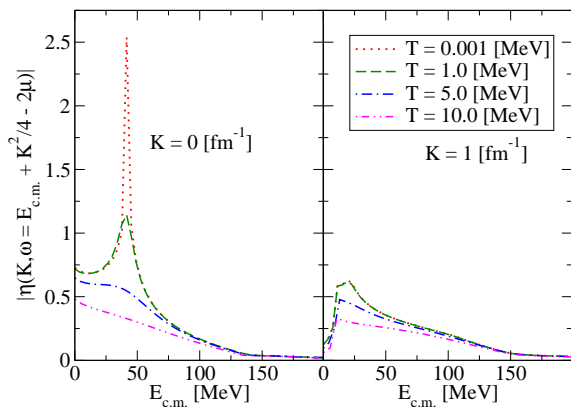


FIG. 1: (color online) Finite temperature Weinberg eigenvalues: Largest eigenvalue as a function of center of mass energy $E_{cm} = E - K^2/4$ for different temperatures T and fixed $\mu = 0.5 \text{ fm}^{-2}$. The left panel corresponds to a center-of-mass momentum $K = 0 \text{ fm}^{-1}$, the right one to $K = 1.0 \text{ fm}^{-1}$.

where the angle-averaged finite-temperature Pauli-blocking factor $\bar{Q}(K, q)$ is given by

$$\bar{Q}(K, q) = \frac{2T}{Kq} \log \left(\frac{1 + e^{\beta[(K/2+q)^2 - 2\mu]/2}}{1 + e^{\beta[(K/2-q)^2 - 2\mu]/2}} \right) - 1. \quad (8)$$

Pairing usually manifests itself as an instability in the two-particle Green's function or the T matrix [15, 23, 24]. At zero temperature, the eigenvalues for $K = 0$ diverge as $E \rightarrow 2\mu$ and cross 1 at energy $E = 2\mu \pm \Delta$, where Δ is the zero-temperature pairing gap [23]. Analogously, at finite temperature, setting the momentum of the center of mass $K = 0$ and the energy $E = 2\mu$, one expects at least one eigenvalue to cross 1 in Eq. (6). The temperature corresponding to such a crossing is the critical temperature T_c marking the on-set of the transition from the normal phase to the paired phase.

This is illustrated in Figs. 1 and 2. In our calculations, we use matrix elements $v(q, q')$ from [28] that were obtained from the AV₁₈ interaction with a smooth regulator (F.D. regulator $\epsilon = 0.5$) at a cutoff of $\Lambda = 2 \text{ fm}^{-1}$ unless otherwise stated.

Fig. 1 shows the magnitude of the largest finite temperature eigenvalue as a function of center of mass energy for different values of the center of mass momentum K . Note that for low temperatures, when $K = 0$, the eigenvalue shows a singular behavior close to the Fermi surface, i.e., at $E = 2\mu$, which signals the pairing instability. Increasing the temperature T or the total momentum K , the Pauli blocking factor gets smeared and the eigenvalues are no longer singular. The largest Weinberg eigenvalue as a function of temperature for energy $E = 2\mu$ and center of mass momentum $K = 0$ is shown in Fig. 2. The temperature at which the eigenvalue equals 1 is the critical temperature (for example, the transition temperature for $\mu = 0.25 \text{ fm}^{-2}$ is indicated by an arrow in the figure).

Fig. 3 shows the transition temperature T_c , determined

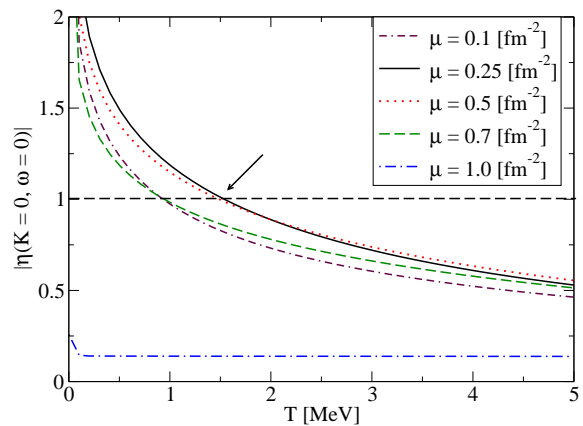


FIG. 2: (color online) Finite temperature Weinberg eigenvalues: Largest eigenvalue for $E = 2\mu$ and $K = 0$ as a function of T for different values of the chemical potential μ . The temperature where the eigenvalue crosses 1 (horizontal dashed line) corresponds to the critical temperature T_c .

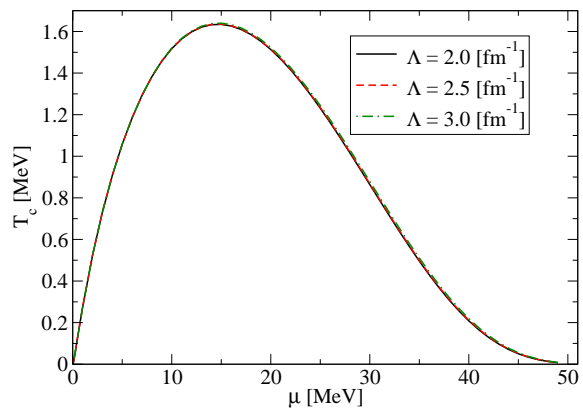


FIG. 3: (color online) Transition temperature as a function of μ obtained from the pole in the T matrix, for different values of the cutoff ($\Lambda = 2, 2.5$ and 3 fm^{-1}).

from the Weinberg eigenvalues, as a function of μ for different cutoffs Λ between 2 and 3 fm^{-1} . The observed cutoff independence is probably a peculiarity of the present approach to calculate T_c from the ladder diagrams with a free single-particle spectrum, the only many-body effect being Pauli blocking that is not affected by the truncation of the model space (as long as the cutoff is above k_F).

In the next section, we set up the correlated density in the Weinberg eigenvector basis and this allows one to generalize the NSR approach to non-local and non-separable interactions.

III. WEINBERG EIGENVALUES AND THE NOZIÈRES-SCHMITT-RINK APPROACH

The NSR approach [15] accounts for the fact that there can be strong pair correlations already above the transition temperature T_c . Although there is no bound di-neutron, the presence of the surrounding medium induces strong correlations and one sometimes speaks of “pre-formed pairs” that are similar to Cooper pairs, but not yet condensed into the $K = 0$ state. A very similar approach was developed by the Rostock group [9, 10], where it was pointed out that one should think of the entire picture in terms of free and correlated quasiparticles instead of free and correlated neutrons. Here, we will suppose that the quasiparticle dispersion relation $\epsilon_{\mathbf{k}}$ is, up to a possible constant shift that can be absorbed in the chemical potential, close to the free one, $\epsilon_{\mathbf{k}} \approx k^2/2$. The effect of the modification of the momentum dependence of the quasiparticle dispersion (effective mass) on the BCS gap, calculated within the Hartree-Fock (HF) approximation using chiral low-momentum interactions including three-body force, was studied in [29] and it was found that this effect is very weak at low densities (see Fig. 10 of [29]).

Within the NSR approach, the density of neutrons at finite temperatures can be decomposed into the following pieces:

$$\rho = \rho_{\text{free}} + \rho_{\text{corr}}. \quad (9)$$

The first term, ρ_{free} , is the density of uncorrelated neutrons,

$$\rho_{\text{free}} = 2 \int \frac{d^3k}{(2\pi)^3} f(\xi_{\mathbf{k}}), \quad (10)$$

where the factor of 2 accounts for the spin degeneracy. The second term, ρ_{corr} , is the contribution due to two neutron scattering and is given by

$$\rho_{\text{corr}} = 2 \int \frac{d^3k}{(2\pi)^3} \frac{1}{\beta} \sum_{\omega_n} \left(\mathcal{G}_0^{(1)}(\mathbf{k}, \omega_n) \right)^2 \Sigma(\mathbf{k}, \omega_n), \quad (11)$$

The single-particle self-energy Σ (see Fig. 4) is calculated in ladder approximation, i.e.,

$$\Sigma(\mathbf{k}, \omega_n) = \int \frac{d^3K}{(2\pi)^3} \frac{1}{\beta} \sum_{\omega_N} \mathcal{G}_0^{(1)}(\mathbf{K} - \mathbf{k}, \omega_N - \omega_n) \times T\left(\mathbf{K}, \frac{\mathbf{K}}{2} - \mathbf{k}, \frac{\mathbf{K}}{2} - \mathbf{k}, \omega_N\right), \quad (12)$$

with the neutron-neutron T matrix that satisfies the following equation:

$$T(\mathbf{K}, \mathbf{q}, \mathbf{q}', \omega_N) = V(\mathbf{q}, \mathbf{q}') + \int \frac{d^3q''}{(2\pi)^3} V(\mathbf{q}, \mathbf{q}'') \mathcal{G}_0^{(2)}(\mathbf{K}, \mathbf{q}'', \omega_N) V(\mathbf{q}'', \mathbf{q}') + \dots \quad (13)$$

Substituting Eq. (12) into Eq. (11) and using $(\mathcal{G}_0^{(1)})^2 = -\partial \mathcal{G}_0^{(1)} / \partial \mu$, we get

$$\rho_{\text{corr}} = -2 \int \frac{d^3K}{(2\pi)^3} \frac{1}{\beta} \sum_{\omega_N} \int \frac{d^3q}{(2\pi)^3} \frac{1}{\beta} \sum_{\omega_n} \left(\frac{\partial}{\partial \mu} \mathcal{G}_0^{(1)}\left(\frac{\mathbf{K}}{2} + \mathbf{q}, \omega_n\right) \right) \mathcal{G}_0^{(1)}\left(\frac{\mathbf{K}}{2} - \mathbf{q}, \omega_N - \omega_n\right) T(\mathbf{K}, -\mathbf{q}, -\mathbf{q}, \omega_N). \quad (14)$$

Next we expand the T matrix in a partial-wave basis and pick out the s -wave ($l = 0$) contribution:

$$T(\mathbf{K}, -\mathbf{q}, -\mathbf{q}, \omega_N) = 4\pi T_{l=0}(K, q, q, \omega_N). \quad (15)$$

Since we can replace \mathbf{q} by $-\mathbf{q}$ in Eq. (14), the derivative $\partial/\partial\mu$ can act on either of the Green's functions $\mathcal{G}_0^{(1)}$ and we can therefore let it act on both if we multiply by a factor of $\frac{1}{2}$. Using the definition (4), we may therefore write

$$\rho_{\text{corr}} = \int \frac{d^3K}{(2\pi)^3} \frac{1}{\beta} \sum_{\omega_N} \int \frac{d^3q}{(2\pi)^3} \left(\frac{\partial}{\partial \mu} \mathcal{G}_0^{(2)}(\mathbf{K}, \mathbf{q}, \omega_N) \right) \times T_{l=0}(K, q, q, \omega_N). \quad (16)$$

Now we rewrite also Eq. (13) in a partial-wave basis and insert it into Eq. (16). Since we consider only the s wave,

we may replace $\mathcal{G}_0^{(2)}$ by its angle average $\overline{\mathcal{G}}_0^{(2)}$. In an analogous way as explained above, we account for the derivative $\partial/\partial\mu$ acting on all the $\overline{\mathcal{G}}_0^{(2)}$ if we multiply the i -th term by a factor $\frac{1}{i}$:

$$\rho_{\text{corr}} = \frac{\partial}{\partial \mu} \int \frac{K^2 dK}{2\pi^2} \frac{1}{\beta} \sum_{\omega_N} \left[\frac{2}{\pi} \int q^2 dq \overline{\mathcal{G}}_0^{(2)}(q) v(q, q) + \frac{1}{2} \frac{2}{\pi} \int q^2 dq \frac{2}{\pi} \int q'^2 dq' \overline{\mathcal{G}}_0^{(2)}(q) v(q, q') \overline{\mathcal{G}}_0^{(2)}(q') v(q', q) + \dots \right]. \quad (17)$$

For brevity, the arguments K and ω_N have been dropped in $\overline{\mathcal{G}}_0^{(2)}$. The terms in the square brackets can be summed

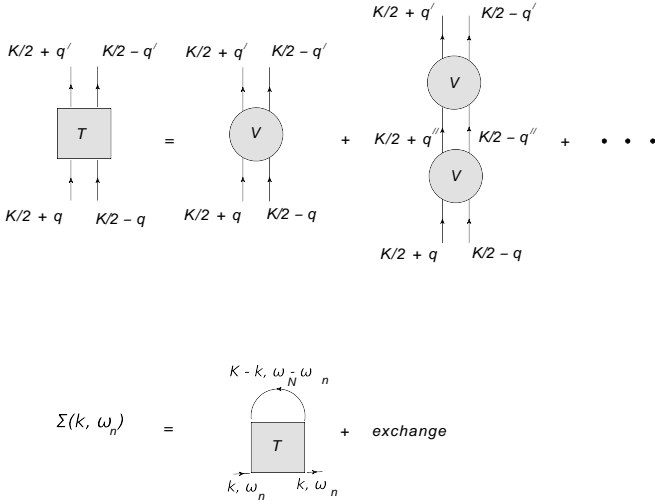


FIG. 4: Feynman Diagrams for the T matrix and the self energy.

so that

$$\rho_{\text{corr}} = -\frac{\partial}{\partial \mu} \int \frac{K^2 dK}{2\pi^2} \frac{1}{\beta} \sum_{\omega_N} \text{Tr} \log \left(1 - \overline{G}_0^{(2)} v \right), \quad (18)$$

where the trace corresponds to the integral over q , the product $\overline{G}_0^{(2)} v$ has to be understood as a product of matrices having continuous indices q, q' , and the logarithm is a matrix logarithm defined by its power series.

Using an analytic continuation as in Eq. (5) and standard techniques to transform the frequency sum into an integral over real energies [27], we obtain

$$\rho_{\text{corr}} = -\frac{\partial}{\partial \mu} \int \frac{K^2 dK}{2\pi^2} \int \frac{d\omega}{\pi} g(\omega) \times \text{Im Tr} \log \left(1 - \overline{G}_0 v \right), \quad (19)$$

where \overline{G}_0 is the retarded two-body Green's function given in Eq. (7) and $g(\omega) = 1/(e^{\beta\omega} - 1)$ is the Bose function. Note that in spite of the pole of the Bose function the integrand is well behaved at $\omega = 0$ because $\overline{Q}(K, q)$ vanishes at $K^2/4 + q^2 = 2\mu$ and therefore $\text{Im} \overline{G}_0$ vanishes at $\omega = 0$. Since the trace is invariant under a change of the basis, it is most convenient to calculate it in the basis of Weinberg eigenvectors where $\overline{G}_0 v$ is diagonal. In this way we get

$$\rho_{\text{corr}} = -\frac{\partial}{\partial \mu} \int \frac{K^2 dK}{2\pi^2} \int \frac{d\omega}{\pi} g(\omega) \times \text{Im} \sum_{\nu} \log \left(1 - \eta_{\nu}(K, \omega) \right). \quad (20)$$

The expression (11) for ρ_{corr} corresponding to the original NSR scheme [15] does not only describe the effect of correlations. A non-vanishing real part of the on-shell self-energy shifts the quasiparticle energies and thereby

strongly affects the density at fixed chemical potential. However, there is no reason to assume that the shift calculated with only the two-body interaction in the 1S_0 channel is realistic, and as mentioned before, this shift should be already included in the quasiparticle dispersion relation $\epsilon_{\mathbf{k}}$. One should therefore subtract the real part of the on-shell self-energy $\Sigma^R(\mathbf{k}, \xi_{\mathbf{k}})$ [where Σ^R denotes the retarded self-energy, related to the imaginary-time self-energy Σ of Eq. (12) by analytic continuation] from the self-energy in Eq. (11). This prescription was used in symmetric matter [9–11], see appendix for more details. In the present work, we will use a slightly simplified prescription, namely we will subtract only the energy-independent leading term of the self-energy,

$$\Sigma_1(\mathbf{k}) = \int \frac{d^3 p}{(2\pi)^3} V\left(\frac{\mathbf{k}-\mathbf{p}}{2}, \frac{\mathbf{k}-\mathbf{p}}{2}\right) f(\xi_{\mathbf{p}}). \quad (21)$$

This corresponds to the HF potential, except that it is not calculated self-consistently. The change in density due to Σ_1 is given by

$$\rho_1 = 2 \int \frac{d^3 k}{(2\pi)^3} \frac{\partial f(\xi_{\mathbf{k}})}{\partial \xi_{\mathbf{k}}} \Sigma_1(\mathbf{k}). \quad (22)$$

With the help of the property $f(\xi_{\mathbf{k}})f(\xi_{\mathbf{p}}) = g(\xi_{\mathbf{k}+\xi_{\mathbf{p}}})[1 - f(\xi_{\mathbf{k}}) - f(\xi_{\mathbf{p}})]$ and after transformation to total and relative momenta, this can be rewritten in a form with no angular integrals as

$$\rho_1 = -\frac{\partial}{\partial \mu} \int \frac{K^2 dK}{2\pi^2} \frac{2}{\pi} \int q^2 dq g\left(\frac{K^2}{4} + q^2 - 2\mu\right) \times v(q, q) \overline{Q}(K, q), \quad (23)$$

The corrected correlated density is now given by $\rho_{\text{corr}} - \rho_1$.

We have seen that the use of the Weinberg eigenvector basis, where $\overline{G}_0 v$ is diagonal, offers a convenient way to apply the NSR scheme to the case of a non-local and non-separable interaction, such as the low-momentum interaction $V_{\text{low } k}$. We can now study the total density at different temperatures above the transition temperature and analyze the importance of correlations. We present our results in the next section.

IV. RESULTS AND DISCUSSION

In section II we presented a method to obtain the transition temperature T_c as a function of the chemical potential μ using the Weinberg eigenvalues. In BCS theory, one assumes that there are no correlations above T_c , and therefore one computes the transition temperature as a function of the density ρ by using $\rho = \rho_{\text{free}}$ according to Eq. (10). However, as discussed in the preceding section, the presence of correlated pairs above T_c changes the relation between μ and ρ . In Fig. 5, we show our results for the correlated density ρ_{corr} at the transition temperature T_c with (upper panel) and without (lower panel) the

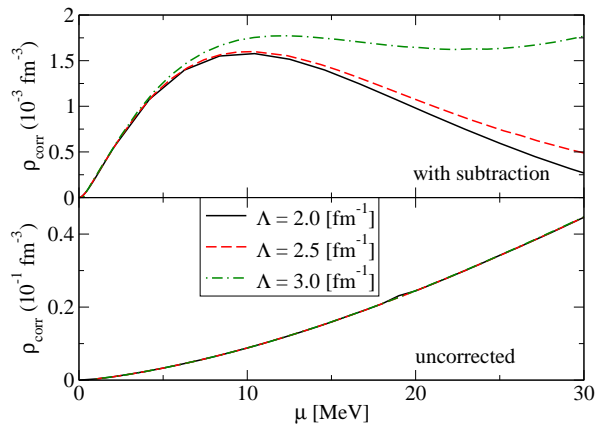


FIG. 5: (color online) Correlated density ρ_{corr} at $T = T_c(\mu)$ with (upper panel) and without (lower panel) the correction (23) as functions of the chemical potential μ . The different curves were obtained with $V_{\text{low } k}$ interactions corresponding to cutoffs $\Lambda = 2, 2.5, \text{ and } 3 \text{ fm}^{-1}$.

subtraction of the contribution due to the HF like shift, Eq. (23), as functions of the chemical potential μ . We observe that without the subtraction, ρ_{corr} is monotonically increasing, while the subtraction reduces it a lot, especially at large μ (high density). We did the calculations for different values of the cutoff Λ between 2 and 3 fm^{-1} , and as it was the case for T_c (cf. Fig. 3), the cut-off dependence of ρ_{corr} without the correction for the HF like shift is very weak. Therefore, one can conclude that the correlated density without the subtraction as defined in III is well constrained by the NN phase shift analogous to the transition temperature T_c . Such weak cut-off dependence was already seen in the BCS pairing gaps in [17]. However, we note that the corrected densities depend on the cutoff, especially at high density. This dependence can be traced back to the HF approximation of the subtracted on-shell self energy. Only with low cutoffs where the interaction has been sufficiently softened, will the HF self-energy subtraction suffice, while in the case of $\Lambda = 3 \text{ fm}^{-1}$ the correlated density ρ_{corr} does not vanish at large μ (i.e., high density). The cut-off dependence of the HF contribution at high density is an indication for missing three-body and other higher order effects.

Fortunately, at the densities where the cutoff dependence from this correction is significant, the total density is completely dominated by the free one. Therefore, the total density is only weakly cutoff dependent. This can be better understood from Fig. 6, where we show the ratio $\rho_{\text{corr}}/\rho_{\text{free}}$ of the correlated density at $T = T_c$ to the free density as a function of the chemical potential μ , again for cutoffs $\Lambda = 2, 2.5, \text{ and } 3 \text{ fm}^{-1}$. The figure also shows the effect of the HF like subtraction. The lower curves are the ratios calculated with the subtraction (23), while the upper curve does not have the correction. Without the subtraction, we can clearly see the over-all change of the densities due to the HF like shift of the quasi-particle

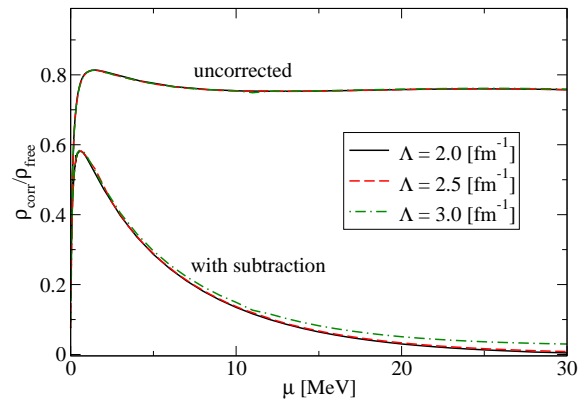


FIG. 6: Ratio of the correlated density to the free density ($\rho_{\text{corr}}/\rho_{\text{free}} = \rho/\rho_{\text{free}} - 1$) as function of the chemical potential μ at $T = T_c(\mu)$ with (lower curves) and without (upper curve) the subtraction term (23). The different curves correspond to cut-offs $\Lambda = 2, 2.5, \text{ and } 3 \text{ fm}^{-1}$. We see that the cut-off dependence is drastically lowered as compared to the upper panel of Fig. 5 because of the dominant contribution from the free density.

energies. Once we include the subtraction, the densities converge towards the free ones in the limit of large μ , i.e., at high densities. This shows clearly that at high densities the shift comes only from the first-order (HF like) term and has nothing to do with correlated pairs. This was expected, since at high densities, pair correlations are weak, as one can see from the low critical temperature in Fig. 3. However, at low densities, the correlations lead to a sizeable enhancement of the density. In other words, if one fixes the density ρ , the correlations lead to a reduction of the chemical potential μ . This results in a reduction of the critical temperature T_c as a function of ρ with respect to the BCS one.

This brings us to the main result of our study, namely the density dependence of the transition temperature, displayed in Fig. 7. The BCS result, obtained with $\rho(\mu) = \rho_{\text{free}}(\mu)$, is shown as the dotted line. If we calculate the total density according to Eq. (9), including the correction in Eq. (23), we obtain the NSR results shown as the solid, dashed, and dashed-dotted lines (corresponding again to the three cutoffs $\Lambda = 2, 2.5, \text{ and } 3 \text{ fm}^{-1}$) We note that the BCS and NSR results agree above $k_F \sim 0.8 \text{ fm}^{-1}$, i.e., at densities above $0.017 \text{ fm}^{-3} \sim 0.1\rho_0$ ($\rho_0 = 0.17 \text{ fm}^{-3}$ being the saturation density of nuclear matter), as one could have anticipated from the vanishing of ρ_{corr} at high density. Notice that within the original NSR scheme, i.e., without the subtraction of Eq. (23), this would not have been the case. At lower densities, the NSR transition temperature is significantly lower than the BCS one. Not surprisingly, the pair correlations above T_c are most important at low densities, where the neutron gas is in the BCS-BEC crossover regime close to the unitary limit.

For comparison we show as the dashed-double dot-

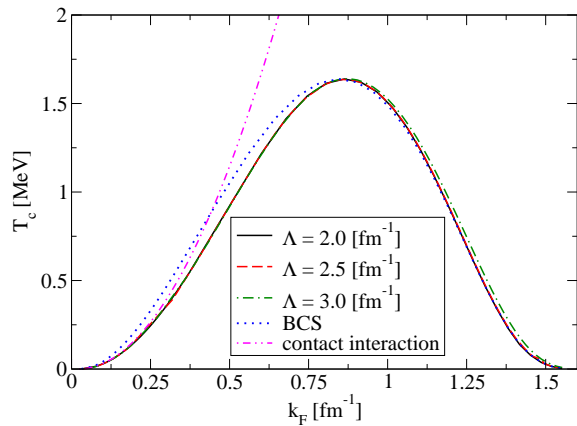


FIG. 7: (color online) Transition temperature T_c as a function of $k_F = (3\pi^2\rho)^{1/3}$. Solid, dashed, and dashed-dotted lines: full NSR results with correction obtained with $V_{\text{low } k}$ interactions corresponding to cutoffs $\Lambda = 2, 2.5$ and 3 fm^{-1} ; dotted line: corresponding BCS results ($\rho = \rho_{\text{free}}$); dashed-double dotted line: result for a contact interaction corresponding to a scattering length $a = -18 \text{ fm}$ within the original NSR scheme [30].

ted line the results obtained within the NSR scheme with a contact interaction [30]. The contact interaction is characterized by the scattering length that is set to $a = -18 \text{ fm}$. By fixing the scattering length, the coupling constant and the cutoff are related, and when one takes the cutoff to infinity the coupling constant goes to zero. Therefore there is no correction from the subtraction of the first-order (HF like) contribution in this scheme. We see that the results of the full calculation are in good agreement with the results for the contact interaction up to $k_F \sim 0.2 \text{ fm}^{-1}$, i.e., only up to a tiny density of $\sim 0.0003 \text{ fm}^{-3} \sim 0.002\rho_0$. At higher densities, the combination of the finite range of the interaction and Pauli blocking leads to a suppression of pairing correlations.

By comparing the results obtained with different cutoffs (solid, dashed, and dashed-dotted curves in Fig. 7), one observes a weak cut-off dependence that arises at high densities. This sets the scale for the missing higher-order contributions as well the missing three and higher-body forces. Analogous to Fig. 5, we see that the cut-off dependence is weak as it is overwhelmed by the contributions from ρ_{free} at high densities due to Pauli blocking. The cut-off dependence seen here will be different if one were to, for example, include corrections to the quasi-particle energies. These effects become especially important at high densities [29].

Finally, in order to discuss the connection between low-density neutron matter and the BCS-BEC crossover, we show in Fig. 8 the same results as in Fig. 7, but plotted in a different way. In the case of a contact interaction, the crossover is characterized by the dimensionless parameter $1/(k_F a)$: for $1/(k_F a) \ll -1$, the system is in the BCS

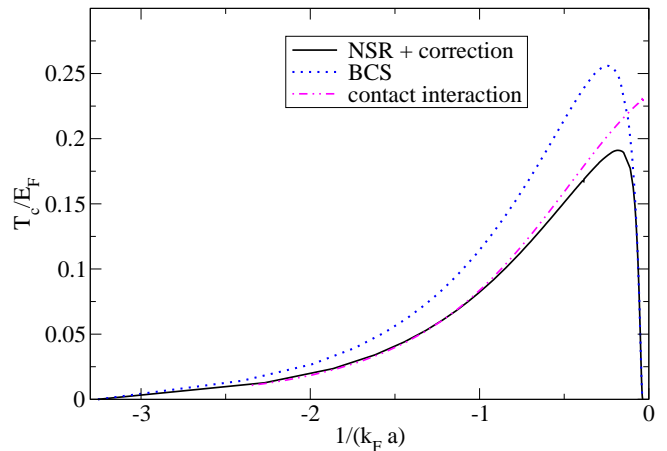


FIG. 8: (color online) Same results as shown in Fig. 7, but T_c is scaled by the Fermi energy $E_F = k_F^2/2$ and shown as function of the dimensionless BEC-BCS crossover parameter $1/(k_F a)$.

regime; for $|1/(k_F a)| \lesssim 1$, the system is in the crossover regime, $1/(k_F a) = 0$ corresponding to the unitary limit; and for $1/(k_F a) \gg 1$, the system forms a BEC of bound dimers. While in experiments with ultracold atoms the whole crossover can be studied by varying a [31, 32], only the region of negative $1/(k_F a)$ is accessible in neutron matter by varying k_F . In Fig. 8 we show the dimensionless ratio T_c/E_F , (E_F being the Fermi energy) in neutron matter within NSR (solid line) and BCS (dotted line) as well as the result for a contact interaction with $a = -18 \text{ fm}$ within the NSR approach (dashed-double dotted line), as functions of $1/(k_F a)$. As we already observed in Fig. 7, the NSR results for the neutron-neutron and contact interactions are in good agreement at very low densities [$1/(k_F a) \lesssim -0.8$], while at $1/(k_F a) \gtrsim -0.1$ the finite range of the neutron-neutron interaction leads to a strong suppression of pairing correlations so that the system returns to the BCS regime. The point where neutron matter is closest to the unitary Fermi gas is $1/(k_F a) \sim -0.2$, corresponding to a very small density of $\sim 0.0007 \text{ fm}^{-3} \sim 0.004\rho_0$.

On a quantitative level, there still remain strong uncertainties. Although we find at low densities a significant reduction of T_c with respect to the BCS result, other many-body effects may lead to additional suppression of T_c . For instance, the inclusion of the HF quasiparticle effective mass, $m^* < m$, reduces the density of states and therefore the critical temperature. In this case, also the cutoff-independence of the results would be lost. Such effects were studied, e.g., in [29], and they are important at higher density, but not in the cross-over region on which we are focusing here. Screening of the interaction by the medium, which is not included in the present calculation either, can also result in a dramatic suppression of pairing [33]. That corrections beyond NSR have to play a role can be seen, for instance, in the case of the

contact interaction in the unitary limit ($a \rightarrow \infty$). In this case, the NSR scheme predicts a critical temperature of $T_c/E_F = 0.23$ [30], which is strongly reduced compared with the corresponding BCS result of $T_c = 0.49E_F$, but still higher than the experimental value $T_c = 0.167E_F$ measured in an ultracold gas of trapped ${}^6\text{Li}$ atoms [34]. These numbers suggest that, in the case of a contact interaction near the unitary limit, the NSR scheme is able to describe the essential effect. However, it is possible that in neutron matter, where the interaction is much more complex than in ultracold atoms, screening corrections might be more important. This question needs further investigations.

V. SUMMARY AND OUTLOOK

In this paper, we study the effect of correlations above the superfluid transition temperature in neutron matter in the BEC-BCS crossover regime within the Nozières-Schmitt-Rink scheme. We use as input the renormalization group based low-momentum effective interaction $V_{\text{low } k}$. In order to deal with the non-local interaction, we use the Weinberg basis, where the operator G_0V is diagonal. Our results show that the transition temperature is lower than the BCS result at low densities, while at high densities we get back the BCS result. At very low densities, our results are in reasonable agreement with those obtained with a contact interaction.

Our main goal is to demonstrate the importance of beyond BCS physics in neutron matter in the crossover regime, and our study is far from being exhaustive. For instance, we use a free particle spectrum and correct for the constant shift of quasi-particle energies using the static Hartree-Fock approximation. We also neglect three-body forces for the sake of simplicity.

It would certainly be interesting to incorporate a three-body force or at least a density dependent two-body force, although one expects such effects to be important at higher densities [29] where the BCS results hold. A calculation including the three-body force would be far more involved. For example, if one includes a density dependent two-body force, the interaction will have to be evaluated self-consistently as the correlations are built into the total density. Similarly, a subtraction of the full on-shell self-energy within the ladder approximation would reduce the cut-off dependence seen in Figs. 5, 6 and 7, but such a calculation is beyond the scope of the current work, although it is worth-while investigating in future.

Finally, other many-body effects like particle-hole correlations (screening) [33] are also important. In the low-density limit, these effects are known to reduce the critical temperature by a factor of $1/(4e)^{1/3} \approx 0.45$ (Gor'kov-Melik-Barkhudarov correction [35]). Therefore, they should be included in future studies.

Acknowledgments

We would like to thank Peter Schuck for discussions and Dick Furnstahl for comments on the manuscript. SR acknowledges the support and hospitality of IPN Orsay where a major part of the work was carried out. SR also acknowledges the support from the HPC cluster at IIT Madras, Chennai, India.

Appendix: Justification of the subtraction

In this appendix we wish to explain in more detail the necessity of subtracting the mean-field shift from the self-energy when calculating the correlated density. As pointed out in section III, a problem of the original NSR approach [15] is that the self-energy, including its energy-independent part leading to a mean-field-like shift of the single-particle energies, is treated only perturbatively. But the shift of the single-particle energies results in a strong correction of the density which has nothing to do with pair correlations and which in a more consistent calculation would be absorbed to a large extent in a corrected chemical potential.

In the NSR approach, the self-energy Σ is calculated with free propagators $\mathcal{G}_0^{(1)}$ given by Eq. (3). However, in a more complete calculation, one should use (self-consistent) dressed Green's functions

$$\mathcal{G}^{(1)}(k, \omega_n) = \frac{1}{i\omega_n - \xi_k - \Sigma(k, \omega_n)} \quad (\text{A.1})$$

throughout the calculation of Σ . Since this is very difficult, one should at least approximate the dressed Green's functions by quasiparticle ones

$$\tilde{\mathcal{G}}_0^{(1)}(k, \omega_n) = \frac{1}{i\omega_n - \tilde{\xi}_k} \quad (\text{A.2})$$

where the quasiparticle energy $\tilde{\xi}_k$ includes the shift due to the real part of the self-energy and is determined self-consistently as the solution of

$$\tilde{\xi}_k = \xi_k + \text{Re} \Sigma^R(k, \tilde{\xi}_k). \quad (\text{A.3})$$

Applying the BCS approximation within this quasiparticle picture, the critical temperature T_c is determined from the pole in the T matrix, calculated with $\tilde{\mathcal{G}}_0^{(1)}$ instead of $\mathcal{G}_0^{(1)}$, and the density ρ from Eq. (10) with $\tilde{\xi}_k$ instead of ξ_k . The main effect of replacing particles by quasiparticles comes from the effective mass [$m^* = k_F / (d\tilde{\xi}_k/dk)_{k=k_F}$], since it changes the density of states, while a momentum-independent shift of the single-particle energies has no effect at all on the relation between T_c and ρ since it can be absorbed in an effective chemical potential μ^* .

Let us now go beyond the BCS approximation. In the approach developed in Ref. [36] in the context of solid-

state physics and applied to nuclear matter in Refs. [9–11], only the correlation contribution, i.e., the energy-dependent part of the self-energy, is treated perturbatively. Then the approximation for the corrected single-particle Green's function reads

$$\mathcal{G}^{(1)}(k, \omega_n) = \tilde{\mathcal{G}}_0^{(1)}(k, \omega_n) + \left(\tilde{\mathcal{G}}_0^{(1)}(k, \omega_n) \right)^2 \left(\Sigma(k, \omega_n) - \text{Re} \Sigma^R(k, \tilde{\xi}_k) \right). \quad (\text{A.4})$$

Note that $\text{Re} \Sigma^R(k, \tilde{\xi}_k)$ has to be subtracted from $\Sigma(k, \omega_n)$ since it is already contained in $\tilde{\mathcal{G}}_0^{(1)}$. The density is now obtained by summing $\mathcal{G}^{(1)}(k, \omega_n)$ over ω_n and integrating over \mathbf{k} , which gives an equation for ρ_{corr} analogous to Eq. (11) but with a subtraction term.

To arrive at the subtraction we use in section III, two additional approximations are made. First, we assume that the single-particle spectrum $\tilde{\xi}_k$ can be approximated by $\tilde{\xi}_k \approx \epsilon_k - \mu^*$, i.e., we neglect the effective mass and other more complicated momentum dependences of

$\text{Re} \Sigma^R(k, \tilde{\xi}_k)$. As it was shown in [29] (where $\tilde{\xi}_k$ was calculated in the HF approximation), these effects are not important in the low-density region we focus on. Note that now the quantity called μ in sections II–IV is not the real chemical potential but the effective one, μ^* , which includes the mean-field shift.

Second, we replace $\text{Re} \Sigma^R(k, \tilde{\xi}_k)$ in the subtraction term by the first-order (HF) term $\Sigma_1(k)$, Eq. (21). The reason for this is a purely practical one. While in the case of a separable potential the correlated density with subtraction can be reduced to a simple expression containing only the in-medium scattering phase shift [9–11, 36], we did not succeed to derive an analogous formula in the case of our non-separable interaction. The direct calculation of the on-shell self-energy $\Sigma^R(k, \tilde{\xi}_k)$, however, is numerically quite involved. This approximation to replace $\text{Re} \Sigma^R(k, \tilde{\xi}_k)$ by $\Sigma_1(k)$ is not valid for large cut-offs and this is the main reason for the cutoff dependence of our results with subtraction.

-
- [1] J. Margueron, H. Sagawa and K. Hagino, Phys. Rev. C **76**, 064316 (2007).
- [2] M. Baldo, C. Maieron, P. Schuck and X. Vinas, Nucl. Phys. A **736**, 241 (2004).
- [3] C. Monrozeau, J. Margueron and N. Sandulescu, Phys. Rev. C **75**, 065807 (2007).
- [4] D. G. Yakovlev and C. J. Pethick, Ann. Rev. Astron. Astrophys. **42**, 169 (2004).
- [5] K. Hagino, H. Sagawa, J. Carbonell and P. Schuck, Phys. Rev. Lett. **99**, 022506 (2007).
- [6] H. Sagawa and K. Hagino, J. Phys. Conf. Ser. **413**, 012008 (2013).
- [7] H. Sagawa and K. Hagino, e-print arXiv:0709.1310 [nucl-ex] (2007).
- [8] K. Hagino and H. Sagawa, Phys. Rev. C **72**, 044321 (2005).
- [9] M. Schmidt, G. Röpke, and H. Schulz, Ann. Phys. (N.Y.) **202**, 57 (1990).
- [10] H. Stein, A. Schnell, T. Alm, and G. Röpke, Z. Phys. A **351**, 295 (1995).
- [11] M. Jin, M. Urban and P. Schuck, Phys. Rev. C **82**, 024911 (2010).
- [12] G. A. Baker Jr., Phys. Rev. C **60**, 054311 (1999).
- [13] D. E. González Trotter *et al.*, Phys. Rev. Lett. **83**, 3788 (1999).
- [14] N. Chamel and P. Haensel, Living Rev. Relativity **11**, 10 (2008) [<http://www.livingreviews.org/lrr-2008-10>].
- [15] P. Nozières and S. Schmitt-Rink, J. Low Temp. Phys. **59**, 195, (1985).
- [16] S. K. Bogner, R. J. Furnstahl and A. Schwenk, Prog. Part. Nucl. Phys. **65**, 94 (2010) [arXiv:0912.3688 [nucl-th]].
- [17] K. Hebeler, A. Schwenk, and B. Friman, Phys. Lett. B **648**, 176 (2007).
- [18] T. Lesinski, T. Duguet, K. Bennaceur, and J. Meyer, Eur. Phys. J. A **40**, 121 (2009)
- [19] K. Hebeler, T. Duguet, T. Lesinski, and A. Schwenk, Phys. Rev. C **80**, 044321 (2009).
- [20] S. Weinberg, Phys. Rev. **131** 440 (1963).
- [21] S. K. Bogner, R. J. Furnstahl, S. Ramanan, and A. Schwenk, Nucl. Phys. **A773** (2006) 203.
- [22] S. K. Bogner, A. Schwenk, R. J. Furnstahl and A. Nogga, Nucl. Phys. A **763**, 59 (2005) [nucl-th/0504043].
- [23] S. Ramanan, S. K. Bogner, and R. J. Furnstahl, Nucl. Phys. A **797**, 81 (2007).
- [24] D. J. Thouless, Ann. Phys. (N.Y.) **10**, 553 (1960).
- [25] P. Ring and P. Schuck, *The Nuclear Many-Body Problem* (Springer-Verlag, Berlin, 1980).
- [26] W. Glöckle, *The Quantum Mechanical Few-Body Problem* (Springer-Verlag, Berlin, 1983).
- [27] A. L. Fetter and J. D. Walecka, *Quantum Theory of Many-Particle Systems* (McGraw-Hill, New York, 1971).
- [28] S. K. Bogner, R. J. Furnstahl, S. Ramanan, and A. Schwenk, Nucl. Phys. **A784** (2007) 79.
- [29] K. Hebeler and A. Schwenk, Phys. Rev. C **82**, 014314 (2010).
- [30] C. A. R. Sá de Melo, M. Randeria, and J. R. Engelbrecht, Phys. Rev. Lett. **71**, 3202 (1993).
- [31] C. A. Regal, M. Greiner, and D. S. Jin, Phys. Rev. Lett. **92**, 040403 (2004).
- [32] M. W. Zwierlein, C. A. Stan, and C. H. Schunck, S. M. F. Raupach, A. J. Kerman, and W. Ketterle, Phys. Rev. Lett. **92**, 120403 (2004).
- [33] C. Shen, U. Lombardo, P. Schuck, W. Zuo, and N. Sandulescu, Phys. Rev. C **67**, 061302 (2003).
- [34] M. J. H. Ku, A. T. Sommer, L. W. Cheuk, and M. W. Zwierlein, Science **335**, 563 (2012).
- [35] L. P. Gor'kov and T. K. Melik-Barkhudarov, J. Exptl. Theoret. Phys. (U.S.S.R.) **40**, 1452 (1961) [translation: Sov. Phys. JETP **13** 1018 (1961)].
- [36] R. Zimmermann and H. Stolz, Phys. Status Solidi B **131**, 151 (1985).